Opto-Electronics Review

SRH suppression mechanism in a non-equilibrium MWIR HgCdTe photodiode

Małgorzata Kopytko

Institute of Applied Physics, Military University of Technology, gen. Sylwestra Kaliskiego 2, 00 908 Warsaw, Poland

Article info	Abstract
	The operation of narrow-gap semiconductor devices under non-equilibrium mode is used at temperatures where the materials are normally intrinsic. The phenomenon of minority carrier exclusion and extraction was particularly discussed in the case of the suppression of Auger thermal generation in heterojunction photodiodes, especially important in the long-wave infrared range. This paper shows that the reduction of the dark current in the HgCdTe photodiode operating in the mid-wave infrared range is primarily the result of suppression of the Shockley-Read-Hall generation in the non-equilibrium absorber. Under a reverse bias, the majority carrier concentration is held equal to the majority carrier doping level. This effect also leads to a decreased majority carrier population at the trap level and an effective increase in the carrier lifetime. The analysed device was with the following design: p^+-B_p cap-barrier unit, p-type absorber doped at the level of $8 \cdot 10^{15}$ cm^{-3}, and wide-bandgap N^+ bottom contact layer. At room temperature, the lowest dark current density of $3.12 \cdot 10^{-1}$ A/cm^2 was consistent with the theoretically predicted Shockley-Read-Hall suppression mechanism, about two times smaller than for the equilibrium case.

1. Introduction

Three generation-recombination (GR) mechanisms, namely radiative [1], Auger [2], and Shockley-Read-Hall (SRH) [3, 4] limit the minority carrier lifetime in narrow-bandgap semiconductors used to develop mid-wave infrared (MWIR) and long-wave infrared (LWIR) detectors. The first two are fundamental mechanisms that are determined by the semiconductor band structure and the doping level. Humphreys [5] has shown that the radiative minority carrier lifetime depends on the absorption coefficient and the device geometry and can be significantly extended. The photon recycling (PR) effect allows emitted photons to be reabsorbed and create another electron-hole pair. Direct Auger recombination is a non-radiative process involving the interaction of three carriers. When the electron-hole pair recombines, either an electron gains energy to move to a higher level in the conduction band or a hole is pushed deeper into the valence band instead of producing a photon. This is a process that is particularly important in the LWIR range and at high temperatures.

The SRH mechanism, in turn, is not an intrinsic and fundamental process because it depends on the quality of the technology. It occurs at trap levels associated with native defects or residual impurities in semiconductors, as well as with dislocations, particularly troublesome in the case of detectors epilayers grown on lattice-mismatched substrates (e.g., HgCdTe on GaAs or InAsSb on GaAs). One method to increase the SRH lifetime is to minimize the occurrence of the defect by controlling the material growth. Additionally, buffer layers are used on GaAs substrates to reduce mismatch dislocation. An alternative is to passivate the dislocation, thought to be due to a donor-like pipe, with a suitable impurity [6].

These three mentioned GR mechanisms are of particular interest to discuss in the non-equilibrium situation suitable for reverse-biased photodiodes. With an appropriate detector design, minority carriers are essentially excluded from the active volume, setting up the necessary electric field to remove the majority carriers until a total charge neutrality is achieved. At this point, the majority carrier concentration is held equal to the majority carrier doping level. This leads

*Corresponding author at: malgorzata.kopytko@wat.edu.pl

to a suppression of the inter-band Auger generation, which has been discussed many times in the literature [7–9], but also of the SRH generation from the non-equilibrium active volume. This effect is due to a reduced majority carrier population at the SRH level, which results in a reduction in the capture rate of minority carriers.

Furthermore, the removal of minority carriers from the detector absorber also leads to a corresponding reduction of the photon density which results in the phenomenon of negative luminescence [10, 11]. Thus, in this mode of operation, when the internal generation of photons is reduced, the radiative recombination component can be ignored [6].

The first part of the paper includes a theoretical consider-ation of the SRH mechanism for different detector operation modes. It is shown that the SRH generation rate in the diffusion region is reduced when the detector is operated in the non-equilibrium mode. In the second part of the paper, this phenomenon is discussed for an MWIR HgCdTe hetero-structure photodiode grown by metal organic chemical vapour deposition MOCVD. Experimental dark currents are analysed using analytical equations. It is shown that the reduction of the dark current is primarily the result of suppression of the SRH generation in the non-equilibrium absorber.

2. Detector operation modes

Let us compare the relevant GR components for different detector operation modes:
- absorber in equilibrium,
- non-equilibrium absorber,
- fully depleted absorber.

Devices that operate with an absorber in equilibrium are P-on-N photodiode [Fig. 1(a)] and nBn photoconductor [Fig. 1(b)]. The sources of thermal generation are similar in both with the main exception being that the barrier layer architecture can be operated without a built-in depletion region. This gives an advantage of the nBn detector only at low temperatures, where $n_i << N_D$. In a standard P-on-n photodiode, the two SRH components (diffusion and depletion) are related by $G_{SR(Dif)} << G_{SR(Dep)}$, and the presence of the depletion region determines the device performance. At high temperatures, a large number of intrinsically generated carriers significantly exceed the external n-doping ($n = n_i >> N_D$). As a result, there is a high diffusion generation rate which can switch from Auger 1 to SRH depending on the level of doping.

By replacing the narrow-gap injector region with a wide-gap or a degenerately doped contact, the authors will obtain the non-equilibrium P-ν-N photodiode illustrated in Fig. 1(c). Under the reverse bias, the P-ν junction extracts minority holes from the absorber while they are not re-supplied by the ν-N junction, so their concentration drops to almost zero. The absorber is not in equilibrium since the electron concentration must also be decreased to the residual doping level ($n = N_D$) to maintain charge neutrality. This causes an increase in Auger 1 and SRH lifetimes and a corresponding decrease in thermal generation rates.

If the absorber doping thickness product can be sufficiently low, a photodiode can operate with a fully depleted absorber, as shown in Fig. 1(d). Because of the absence of majority carriers, the GR diffusion component is eliminated. The only dark current is due to the SRH generation by defect states, with the main contribution of those located at the intrinsic energy level. When the defect capture time constants for electrons and holes are sufficiently long, the detector current is set by the blackbody radiation of the background and by the detector quantum efficiency. A detector of this type is referred to as background radiation-limited [12].
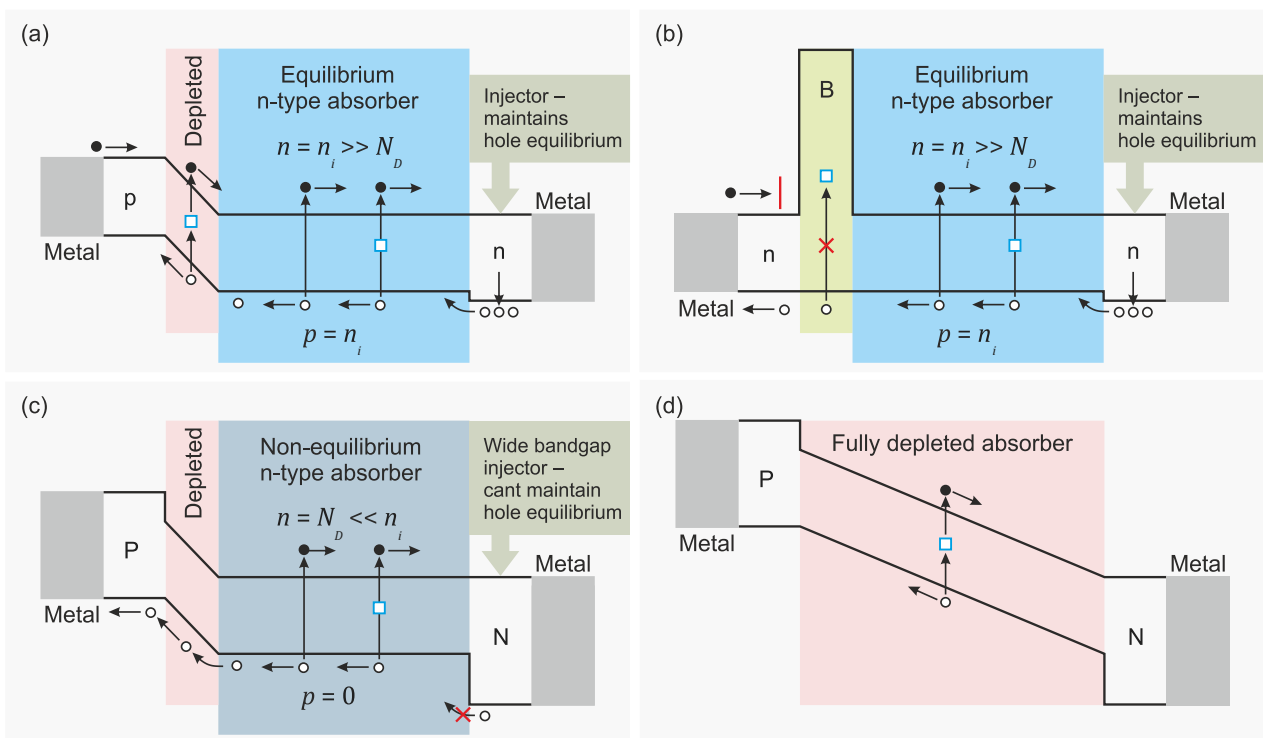
Fig. 1. Comparison of the detector operation modes: P-on-N photodiode (a), nBn photoconductor (b), non-equilibrium P-ν-N photodiode (c), and fully depleted P-ν-N photodiode (d).

It is also interesting to compare temperature dependence of generation rate per unit volume through SRH centres within a field-free region with the generation rate through the same centres located within the depletion region. The expressions for SRH lifetimes in the n-type semiconductor and corresponding generation rates are depicted in Fig. 2. Over the extrinsic to intrinsic temperature range, assuming that $\tau_{p0} = \tau_{n0}$, the equilibrium SRH lifetime exhibits a weak temperature dependence that varies by a factor of 2. For the non-equilibrium absorber, the SRH lifetime exhibits a temperature dependence given by n_i over its intrinsic temperature range. In a depleted region, the effective SRH lifetime is $\tau_{p0} + \tau_{n0}$, as opposed to the lifetime of τ_{p0} in the field-free region and low temperatures.

SRH generation rates *vs.* temperature calculated for n-type MWIR HgCdTe doped at two different levels are presented in Fig. 3. Residual doping of a material determines the temperature transition point between SRH generation from the diffusion region and generation from the depleted region – the lower the doping, the transition point appears at lower temperatures. Over the extrinsic temperature range where $n_i \ll N_D$, generation by the centres located in the depletion region (blue dashed line in Fig. 3) dominates. Over the intrinsic temperature range and equilibrium conditions where $n_i \gg N_D$, the field-free region SRH generation (solid red line) becomes dominant.

However, when the majority carrier concentration is held equal to the doping level, $n = N_D \ll n_i$ (non-equilibrium conditions), the SRH generation (red dotted line) is suppressed and two SRH components – diffusion and depletion – are equal ($G_{SR(Dif)} = G_{SR(Dep)}$), and no penalty is paid for the presence of the depletion region.

3. Analysed photodiode design

The HgCdTe heterostructure was grown in an Aixtron AIX-200 MOCVD system on a 2-in, epi-ready GaAs substrate followed by a 3 μm thick CdTe buffer layer. The analysed HgCdTe photodiode has the following design: p$^+$ B$_p$ cap-barrier unit, p-type absorber, and wide-bandgap N$^+$ bottom contact layer. A 5 μm thick absorber was As-doped at a level of $1 \cdot 10^{16}$ cm^{-3} with a Cd molar composition of 0.28 to obtain a 50% cut-off wavelength of 5.5 μm at 230 K. p$^+$-B$_p$ cap-barrier unit was highly doped with As ($N_A \sim 2 \cdot 10^{17}$ cm^{-3}). The Cd molar content of the cap contact layer was the same as that of the absorber, whereas the barrier was increased to 0.62 to widen the energy gap. A 9 m thick N$^+$ bottom contact layer was highly doped with iodine ($N_D = 2 \cdot 10^{17}$ cm^{-3}) and with a Cd molar composition of 0.55. Due to interdiffusion processes during HgCdTe growth, the x-graded regions were created at heterojunction interfaces.
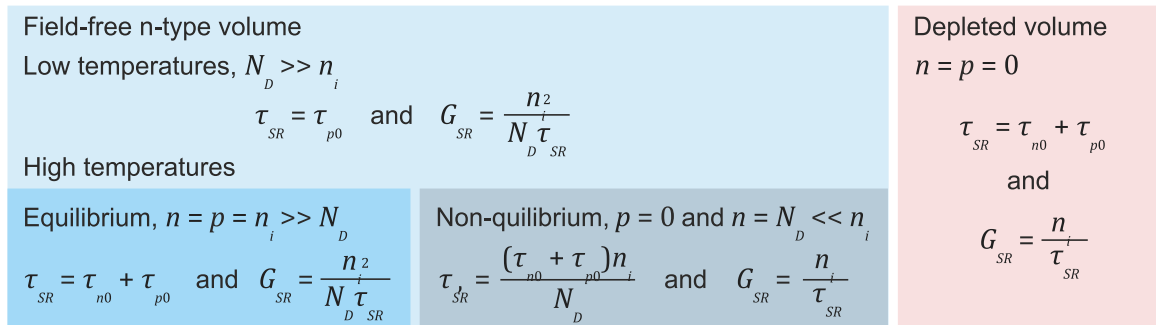

Fig. 2. Comparison of equilibrium and non-equilibrium relationships for carrier lifetimes and generation rates induced by the SRH mechanism in the n-type semiconductor.
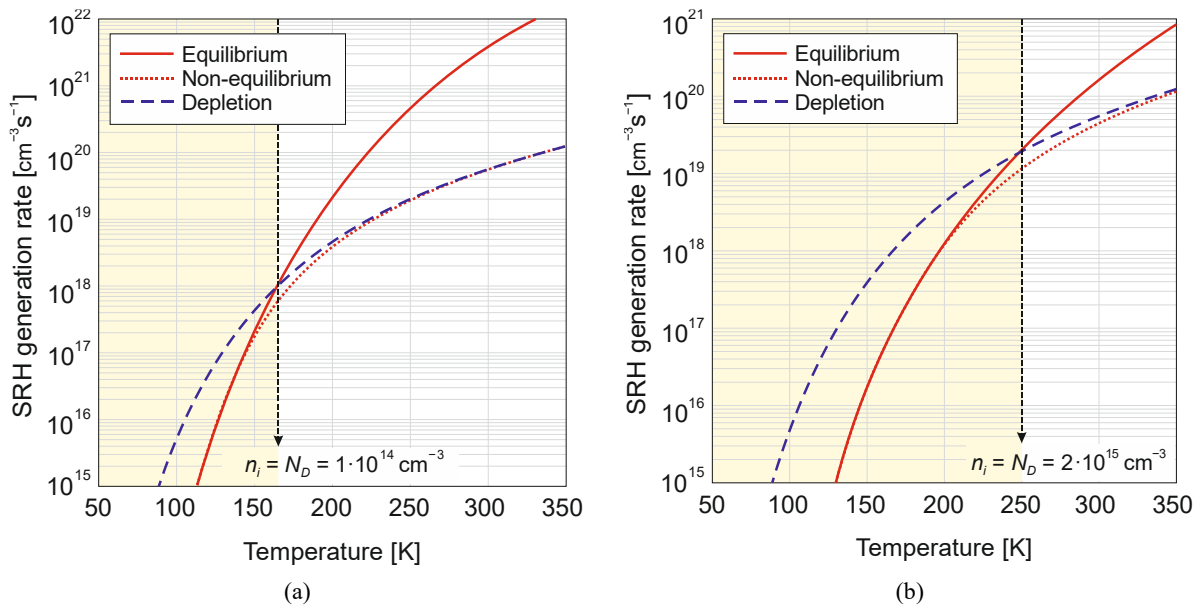

Fig. 3. Calculated SRH generation rate per unit volume *vs.* temperature for an n-type MWIR HgCdTe with Cd molar composition of $x = 0.28$ and a donor doping concentration of $1 \cdot 10^{14}$ cm^{-3} (a) and $2 \cdot 10^{15}$ cm^{-3} (b). Calculations have been done with the assumed value of the defect capture time constants for electrons and holes of $\tau_{n0} = \tau_{p0} = 50$ μs.

Figure 4 shows the schematic design and calculated band profiles for the $p^+B_ppN^+$ photodiode operating at zero and 0.5 V reverse bias voltage and 230 K [13]. Calculations were made with the commercially available software APSYS. At a reverse bias, the absorber and highly doped regions are practically field-free. The space charge region is apparent only at the p-N$^+$ junction, slightly penetrating the absorber region.
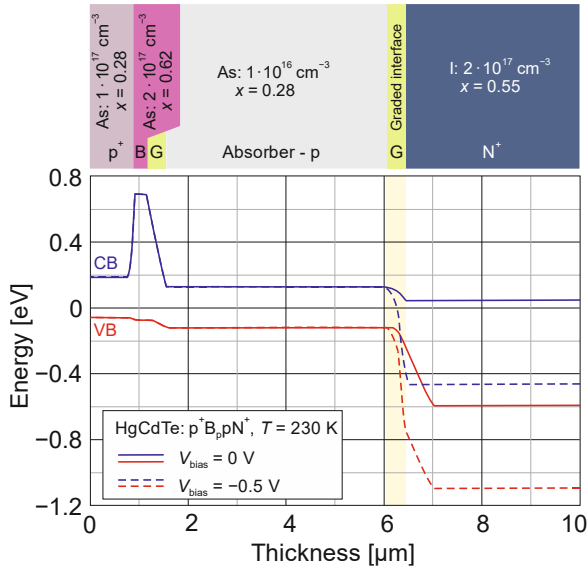

Fig. 4. Calculated band diagrams at 230 K for a HgCdTe heterostructure photodiode operated at zero and reverse bias voltage. After Ref. [13].

4. Results discussion

Diffusion, depletion, and trap assistant tunnelling (TAT) components of a bulk-based model are computed using the equations listed in Appendix 2. The calculations were performed for the equilibrium and non-equilibrium absorbers. In both cases, all assumed parameters were the same and are included in Table 1. To calculate the Auger lifetime, (A1.5) and (A1.8) were used for the equilibrium and non-equilibrium modes, respectively. The diffusion SRH lifetime in equilibrium mode was calculated using (A.12) while in non-equilibrium mode using (A.13). In a depleted region, the SRH lifetime was calculated as $\tau_{SR} = \tau_{p0} + \tau_{n0}$.

Table 1.
Material parameters assumed for calculations.

Parameter	Value
Absorber doping, N_A [cm^{-3}]	$8 \cdot 10^{15}$
Absorber thickness, t_{abs} [μm]	5
Electron effective mass, m_e^*/m_0	0.071 E_g
Hole effective mass, m_{hh}^*/m_0	0.55
Trap concentration, N_T [cm^{-3}]	$2.5 \cdot 10^{13}$
SRH carrier lifetime, τ_{n0}, τ_{p0} [μs]	0.47
Overlap integral, F_1F_2 at 230 K	0.2
Overlap integral, F_1F_2 at 300 K	0.1

Determined by fitting the experimental results for the $p^+B_ppN^+$ photodiode diffusion (equilibrium and non-

equilibrium), and depletion SRH lifetimes *vs*. temperature are shown in Fig. 5. The calculations were made for a constant concentration of traps, set at the level of $N_t = 2.5 \cdot 10^{13}$ cm^{-3} – the same as determined from tunnelling via trap states. Below 150 K, equilibrium and non-equilibrium SRH lifetimes are equal. For $\tau_{p0} = \tau_{n0} = 0.47$ μs, the associated recombination coefficient for the centre is $8.5 \cdot 10^{-8}$ cm^{3}s^{-1}. Between low and high temperatures, the equilibrium SRH lifetime shows a mild temperature dependence, varying by a factor of 2. In turn, the non-equilibrium SRH lifetime increases with increasing temperature. At 300 K, the non-equilibrium SRH lifetime is nearly two times as long as the equilibrium one, which contributes to the reduction of dark currents. The SRH lifetime in the depleted region is constant over the entire temperature range and is 0.94 μs.
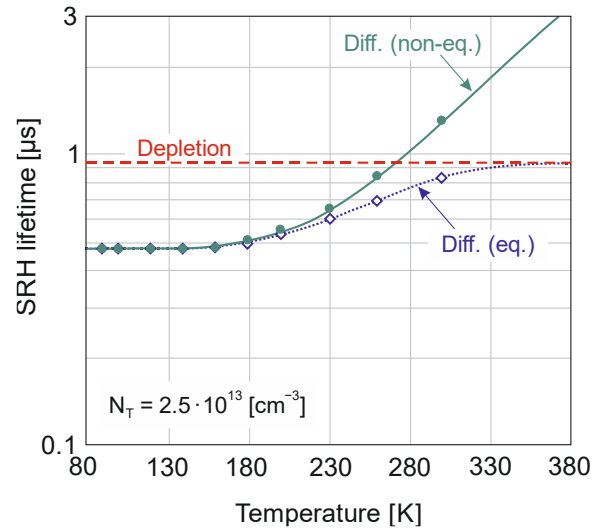

Fig. 5. Equilibrium and non-equilibrium SRH lifetime as a function of temperature-determined based on the fit to experimental results.

Figures 6 and 7 show the dark current analysis performed for the $p^+B_ppN^+$ photodiode at 300 K and 230 K, respectively. Initially, as the reverse bias increases, the current density increases in accordance with theoretical predictions when the material is intrinsic. Next, the breakdown is observed in the characteristics. Intrinsically generated majority carriers are excluded and held equal to the majority carrier doping level – the absorber becomes non-equilibrium, and the saturation current density reduces. At 300 K, the lowest value observed in this device is $3.12 \cdot 10^{-1}$ A/cm^2 for voltages from −0.2 V to −0.4 V. Above −0.2V, the experiment is consistent with the diffusion component which includes Auger and SRH mechanisms. At higher reverse biases, the current increases due to tunnelling through trap states. At 230 K, the current-voltage characteristic is determined by the TAT mechanism in almost the entire range of analysed reverse voltages. The saturation current associated with the diffusion current is visible in the voltage range from −0.1 V to −0.2 V.

The clearest difference between the predictions for the equilibrium and non-equilibrium absorbers is visible at room temperature and results mainly from the suppression of the SRH generation. Almost a double current reduction is due to the decreased hole population of the SRH level, resulting in a decrease in the capture rate of minority carrier

electrons in the non-equilibrium active volume [6]. The suppression of the Auger mechanism under non-equilibrium is also present. However, the diffusion current associated with the Auger mechanism is more than an order of magnitude lower than that of the SRH, therefore the total current is mainly influenced by the latter one. The values of the respective components of the diffusion current density for the voltage of −0.2 V are listed in Table 2.

5. Conclusions

Experimental work on an MWIR HgCdTe p⁺B$_p$pN⁺ photodiode has shown the dark current reduction which is consistent with the theoretically predicted SRH suppression mechanism. This behaviour is observed at high temperatures under the non-equilibrium conditions of minority carrier exclusion in the active volume of the device.
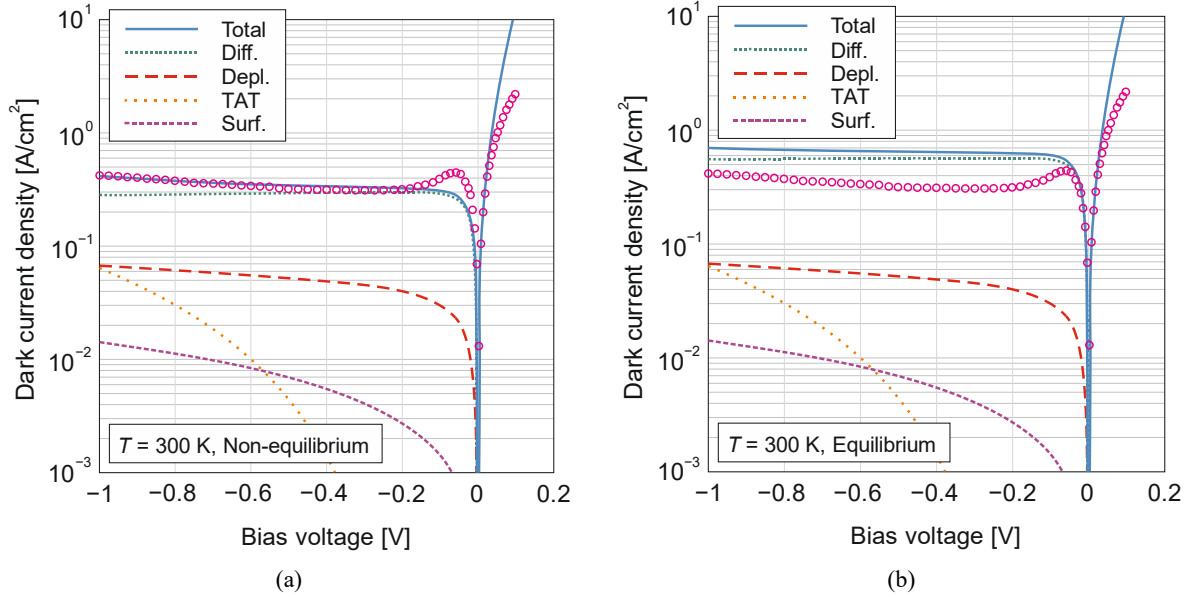

Fig. 6. Experimental (open dots) and simulated (lines) current densities for a HgCdTe heterostructure photodiode with the equilibrium (a) and nonequilibrium (b) absorber at 300 K.
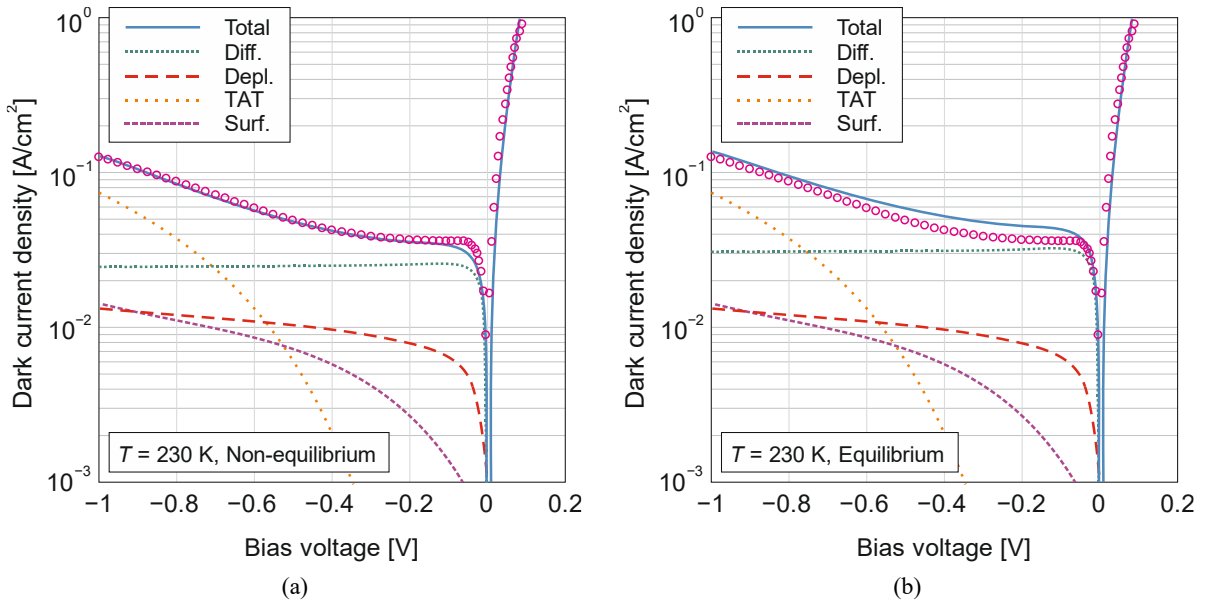

Fig. 7. Experimental (open dots) and simulated (lines) current densities for HgCdTe heterostructure photodiode with the equilibrium (a) and nonequilibrium (b) absorber at 230 K.

Table 2.
Equilibrium and non-equilibrium dark current densities in the MWIR HgCdTe heterostructure photodiode.

U = −0.2 V	J_{dif} (Auger) [A/cm²]		J_{dif} (SRH) [A/cm²]		J_{dif} (Auger+SRH) [A/cm²]	
	Equilibrium	Non-equilibrium	Equilibrium	Non-equilibrium	Equilibrium	Non-equilibrium
300 K	$2 \cdot 10^{-2}$	$1.16 \cdot 10^{-2}$	$5.57 \cdot 10^{-1}$	$3 \cdot 10^{-1}$	$5.77 \cdot 10^{-1}$	$3.12 \cdot 10^{-1}$
230 K	$3.25 \cdot 10^{-3}$	$3.16 \cdot 10^{-3}$	$2.83 \cdot 10^{-2}$	$2.41 \cdot 10^{-2}$	$3.15 \cdot 10^{-2}$	$2.73 \cdot 10^{-2}$

When the HgCdTe $p^+B_ppN^+$ photodiode is reverse biased, the current density initially increases in accordance with theoretical predictions when the material is intrinsic – the equilibrium SRH generation rate is proportional to n_i^2/N_A. When the bias voltage increases and the majority carrier concentration is held equal to the majority carrier doping level, the SRH generation rate is proportional to n_i – the absorber becomes non-equilibrium, and the saturation current density reduces. At 300 K, the lowest value observed in this device is $3.12\cdot10^{-1}$ A/cm² for voltages from −0.2 V to −0.4 V.

Acknowledgements

Appendix 1 – Minority carrier lifetime

According to the van Roosbroeck and Schockley (VRS) expression [1], the internal radiative lifetime is given by

$$\tau_R = \frac{1}{B(n+p)} , \tag{A1.1}$$

where n and p are the electron and hole concentrations, respectively, and

$$B = 5.8 \cdot 10^{-13} \varepsilon_\infty^{1/2} \left(\frac{m_0}{m_e^* + m_{hh}^*}\right)^{3/2}$$
$$\cdot \left(1 + \frac{m_0}{m_e^*} + \frac{m_0}{m_{hh}^*}\right)\left(\frac{300}{T}\right)^{3/2} E_g^2 . \tag{A1.2}$$

ε_∞ is the high frequency permittivity, m_0 is the free electron mass, where m_e^* and m_{hh}^* are the electron and hole effective mass, respectively, and E_g is the semiconductor energy gap at the temperature T.

For n-type material, Auger recombination involves two electrons and one hole – Auger 1 is the primary mechanism, and is given by [14]

$$\tau_{A1} = \frac{2\tau_{Ai1}n_i^2}{n(n+p)} , \tag{A1.3}$$

where n_i is the intrinsic carrier concentration, and τ_{Ai1} is the Auger 1 lifetime for an intrinsic material, expressed as

$$\tau_{Ai1} = 3.8 \cdot 10^{-18}\varepsilon^2(1+\mu)^{1/2}(1+2\mu)\left(\frac{m_0}{m_e^*}\right)$$
$$\cdot \left(\frac{-q(1+2\mu)E_g}{(1+\mu)k_BT}\right)|F_1F_2|^{-2}\left(\frac{k_BT}{qE_g}\right)^{-3/2} , \tag{A1.4}$$

where ε is the dielectric constant, μ is the ratio of the effective masses of the electron and the hole, expressed as m_e^*/m_{hh}^*, q is the free electron charge, k_B is the Boltzmann constant, and F_1F_2 is the overlap integral for Bloch functions. In the Auger model, the final parameter contains the most uncertainty. The values for most narrow-bandgap semiconductors are estimated theoretically to be around 0.25.

For p-type material, Auger 7 which involves two holes and one electron may also be important. It can be expressed by [14]

$$\tau_{A7} = \frac{2\tau_{Ai7}n_i^2}{p(n+p)} , \tag{A1.5}$$

where τ_{Ai7} is Auger 7 lifetime in intrinsic material. It can be expressed by the lifetime determined by Auger 1 process

$$\tau_{Ai7} = \gamma\tau_{Ai1}. \tag{A1.6}$$

Casselman estimated γ to range from 0.5 to 6 [9].
The Auger lifetime in p-type HgCdTe is [15]

$$\tau_A = \frac{\tau_{A1}\tau_{A7}}{\tau_{A1} + \tau_{A7}} , \tag{A1.7}$$

where τ_{A1} and τ_{A7} are described by (A1.3) and (A1.5), respectively.

In non-equilibrium mode, when intrinsically generated majority carriers are excluded and the majority carrier concentration is held equal to the doping level, (A1.3) and (A1.5) become [6]

$$\tau_{A1} = \frac{2\tau_{A7}^i n_i^2}{N_D^2}, \qquad \tau_{A7} = \frac{2\tau_{A7}^i n_i^2}{N_A^2}, \tag{A1.8}$$

for n-type material doped at the level of N_D, and p-type material doped at the level of N_A, respectively.

For a single defect level, the SRH carrier lifetime related to a low-injection level is represented as [3]

$$\tau_{SR} = \frac{\tau_{p0}(n+n_1) + \tau_{n0}(p+p_1)}{n+p}, \tag{A1.9}$$

where τ_{p0} and τ_{n0} are the defect capture time constants for electrons and holes, and

$$n_1 = N_C\exp\left[\frac{(E_T - E_C)}{k_BT}\right],$$
$$p_1 = N_V\exp\left[\frac{(E_V - E_T)}{k_BT}\right], \tag{A1.10}$$

where E_C and E_V are the conduction and valence band edge energies, respectively, and E_T is the SRH defect energy. N_C and N_V are the effective conduction and valence band density-of-states.

The capture time constants τ_{p0} and τ_{n0} are proportional to the inverse product of the defect concentration N_T and the recombination coefficients for electrons and holes, C_n and C_p, respectively, as:

$$\tau_{n0} = (N_TC_n)^{-1}, \quad \tau_{p0} = (N_TC_p)^{-1}. \tag{A1.11}$$

The optimum thermal transition, i.e., the shortest SRH lifetime, occurs through defects located approximately at the intrinsic energy level in the semiconductor bandgap, where $n_1 = p_1 = n_i$.

Then, (A1.9) takes the form

$$\tau_{SR} = \frac{\tau_{p0}(n + n_i) + \tau_{n0}(p + n_i)}{n + p}. \qquad (A1.12)$$

At low temperatures, where $n > n_i$ for n-type semiconductor or $p > n_i$ for p-type semiconductor, the effective SRH lifetime is $\tau_{SR} = \tau_{p0}$ and $\tau_{SR} = \tau_{n0}$, respectively.

At high temperatures, where $n = p = n_i$, the authors have $\tau_{SR} = \tau_{n0} + \tau_{p0}$.

However, under the non-equilibrium mode, (A1.12) takes the form

$$\tau_{SR} = \frac{\tau_{p0}N_D + (\tau_{n0} + \tau_{p0})n_i}{N_D}$$
$$\tau_{SR} = \frac{\tau_{n0}N_A + (\tau_{n0} + \tau_{p0})n_i}{N_A}, \qquad (A1.13)$$

for the n- and p-type active volume.

For the depletion region, where $n = p = 0$, the effective lifetime is $\tau_{SR} = \tau_{n0} + \tau_{p0}$.

Appendix 2 – Dark currents

The dark current-voltage equation for the photodiode is a superposition of several mechanisms [6]

$$J_{bulk} = J_{dif}\left[\exp\left(\frac{qV}{k_BT}\right) - 1\right]$$
$$+ J_{dep}\left[\exp\left(\frac{qV}{2k_BT}\right) - 1\right] - J_T, \qquad (A2.1)$$

where J_{dif} is the diffusion current generated within the electrically neutral region of the absorber within a minority carrier diffusion length, J_{dep} is the depletion current which arises from the space charge region, V is the applied bias, and J_T represent any tunnel [16] due to direct band to band transitions and/or transitions via trap states within the bandgap.

Taking into account Auger and SRH GR mechanisms, the diffusion current density can be expressed as

$$J_{dif} = qtG_{dif} = \frac{qn_i^2t}{N_{maj}}\left(\frac{1}{\tau_A} + \frac{1}{\tau_{SR}}\right), \qquad (A2.2)$$

where t is the diffusion region thickness, G_{dif} is the thermal generation rate per unit volume of minority carriers within a field-free region, N_{maj} is the appropriate majority carrier concentration.

The depletion current density is associated with the SRH mechanism and can be estimated by

$$J_{dep} = qWG_{dep} = \frac{qn_iW}{\tau_{SR}}, \qquad (A2.3)$$

where W is the width of depletion region, and G_{dep} is the steady state GR rate for electrons and holes within the depletion region.

Band to band tunnelling (BtBT) for a parabolic barrier in the uniform electric field ξ is given by [17]

$$J_{BtBT} = \frac{q^3(2m_e^*)^{1/2}\xi V}{4\pi^3\hbar^2E_g^{1/2}}\exp\left(\frac{-\pi m_e^{*1/2}E_g^{3/2}}{2\sqrt{2}q\xi\hbar}\right), \qquad (A2.4)$$

where $\hbar$ is the reduced Planck constant.

TAT through bandgap states is given by [18]

$$J_{TAT} = \frac{q^2m_e^*V\kappa^2N_T}{8\pi\hbar^3(E_g - E_T)}\exp\left(\frac{-m_e^{*1/2}E_g^{3/2}G(a)}{2\sqrt{2}q\xi\hbar}\right), \qquad (A2.5)$$

$$\kappa = \frac{2\sqrt{2\pi}\hbar^2}{m_0}\left(\frac{m_0}{\hbar^2}\right)^{1/4}\frac{E_g}{(0.5E_g)^{3/4}}, \qquad (A2.6)$$

where κ^2 is the matrix element associated with the defect potential, N_T is the density of centres at E_T, and $G(a)$ is the geometrical factor in the exponent.

Appendix 3 – HgCdTe material parameters

A Cd molar composition, x, and a temperature-dependent Hg$_{1-x}$Cd$_x$Te energy gap are given by the empirical relation [19]

$$E_g(x,T) = -0.302 + 1.93x - 0.81x^2$$
$$+ 0.832x^3 + 5.35 \cdot 10^{-4}(1 - 2x)T. \qquad (A3.1)$$

The most widely used expression for the intrinsic carrier concentration in HgCdTe is given by [20]

$$n_i = \begin{pmatrix} 5.585 - 3.82x + 1.753 \cdot 10^{-3}T + \\ +1.364 \cdot 10^{-3}xT \end{pmatrix}$$
$$\cdot 10^{14} E_g^{3/4}T^{3/2}\exp\left(-\frac{E_g}{2k_BT}\right). \qquad (A3.2)$$

In the narrow gap HgCdTe, the electron effective masses can be approximated by $m_e^*/m_0 = 0.071E_g$, while the heavy hole effective mass by $m_{hh}^*/m_0 = 0.55$.

References

[1] Van Roosbroeck, W. & Shockley, W. Photon-radiative recombination of electrons and holes in germanium. *Phys. Rev.* **94**, 1558–1560 (1954). https://doi.org/10.1103/PhysRev.94.1558

[2] Beattie, A. R. & Landsberg, P. T. Auger effect in semiconductors. *Proc. Math. Phys. Eng. Sci.* **249**, 16–29 (1959). https://www.jstor.org/stable/100562

[3] Shockley, W. & Read, W. T. Statistics of recombinations of holes and electrons. *Phys. Rev.* **87**, 835–842 (1952). https://doi.org/10.1103/PhysRev.87.835

[4] Hall, R. N. Electron-hole recombination in germanium. *Phys. Rev.* **87**, 387 (1952). https://doi.org/10.1103/PhysRev.87.387

[5] Humphreys, R. G. Radiative lifetime in semiconductors for infrared detectors. *Infrared Phys.* **26**, 337–342 (1986). https://doi.org/10.1016/0020-0891(86)90054-0

[6] Kinch, M. A. *State-of-the-Art Infrared Detector Technology*. (SPIE Press, Bellingham, 2014). https://doi.org/10.1117/3.1002766

[7] Ashley, T., Elliott, C. T. & Harker, A. T. Non-equilibrium modes of operation for infrared detectors. *Infrared Phys.* **26**, 303–315 (1986). https://doi.org/10.1016/0020-0891(86)90008-4https://doi.org/10.1016/1350-4495(95)00043-7

[8] Elliott, C. T. Non-equilibrium modes of operation of narrow-gap semiconductor devices. *Semicond. Sci. Technol.* **5**, S30–S37 (1990). https://doi.org/10.1088/0268-1242/5/3S/008

[9] Casselman, T. N. Calculation of the Auger lifetime in p-type $Hg_{1-x}Cd_xTe$. *J. Appl. Phys.* **52**, 848 (1981). https://doi.org/10.1063/1.328426

[10] Berdahl, P., Malutenko, V. & Morimoto, T. Negative luminescence of semiconductors. *Infrared Phys.* **29**, 667–672 (1989). https://doi.org/10.1016/0020-0891(89)90107-3

[11] Ashley, T. *et al*. Negative luminescence from $In_{1-x}Al_xSb$ and $Cd_xHg_{1-x}Te$ diodes. *Infrared Phys. Technol.* **36**, 1037–1044 (1995). https://doi.org/10.1016/1350-4495(95)00043-7

[12] Lee, D. *et al*. Law 19 – The ultimate photodiode performance metric. *Proc. SPIE* **11407**, 114070X (2020). https://doi.org/10.1117/12.2564902

[13] Kopytko, M. *et al*. Investigation of syrface leakage current in MWIR HgCDTe and InAsSb barrier detectors. *Semicond. Sci. Technol.* **33**, 125010 (2018). https://doi.org/10.1088/1361-6641/aae768

[14] Blakemore, J. S. *Semiconductor Statistics*. (Pergamon Press, New York, 1962). https://doi.org/10.1016/C2013-0-01678-7

[15] Lopes, V. C., Syllaios, A. J. & Chen, M. C. Minority carrier lifetime in mercury cadmium telluride. *Semicond. Sci. Technol.* **8**, 824 (1993). https://doi.org/10.1088/0268-1242/8/6S/005

[16] Kane, E. O. Theory of tunnelling. *J. Appl. Phys.* **32**, 83–91 (1961). https://doi.org/10.1063/1.1735965

[17] Blanks, D. K., Beck, J. D., Kinch, M. A. & Colombo, L. Band-to-band tunnel processes in HgCdTe: Comparison of experimental and theoretical studies. *J. Vac. Sci. Technol. A* **6**, 2790 (1988). https://doi.org/10.1116/1.575508

[18] Sah, C. T. Electronic processes and excess currents in gold-doped narrow silicon junctions. *Phys. Rev.* **123**, 1594 (1961). https://doi.org/10.1103/PhysRev.123.1594

[19] Hansen, G. L., Schmit, J. L. & Casselman, T. N. Energy gap versus alloy composition and temperature in $Hg_{1-x}Cd_xTe$. *J. Appl. Phys.* **53**, 7099–7101 (1982). https://doi.org/10.1063/1.330018

[20] Hansen, G. L. & Schmit, J. L. Calculation of intrinsic carrier concentration in $Hg_{1-x}Cd_xTe$. *J. Appl. Phys.* **54**, 1639–1640 (1983). https://doi.org/10.1063/1.332153